



Interdecadal modulation of ENSO amplitude by the Atlantic multi-decadal oscillation (AMO)

Yuhan Gong¹ · Tim Li^{1,2} · Lin Chen^{1,3,4}

Received: 27 August 2019 / Accepted: 29 July 2020
© Springer-Verlag GmbH Germany, part of Springer Nature 2020

Abstract

The impact of the Atlantic Multi-decadal Oscillation (AMO) on the ENSO amplitude was investigated through observational analyses. During the past 90 years the interdecadal variability of ENSO intensity is significantly correlated with the AMO. ENSO variability was strengthened (weakened) during a negative (positive) AMO phase. An ocean mixed layer heat budget analysis reveals that the thermocline feedback is the main process regulating AMO negative phase dependent ENSO growth characteristic. A further examination indicates that a strengthened atmospheric response to unit SST anomaly, an enhanced thermocline response to unit wind stress forcing and a strengthened subsurface temperature response to unit thermocline variation all contribute to the enhanced thermocline feedback during the negative phase of AMO. Such changes are attributed to the increase of background moisture, the weakening of mean subtropical cell (STC) and increase of upper ocean vertical temperature gradient respectively.

Keywords AMO · Interdecadal change of ENSO amplitude · Thermocline feedback · Zonal advective feedback · Mixed layer heat budget

1 Introduction

El Niño-Southern Oscillation (ENSO) is the strongest inter-annual variability in the global climate system. It is characterized by a large-scale sea surface temperature (SST)

anomaly pattern in the tropical Pacific and remote precipitation and circulation response in a variety of regions (Ropelewski and Halpert 1989; Philander 1990; Halpert and Ropelewski 1992). The structure and evolution characteristics of ENSO has been described by many previous studies (e.g., Rasmusson and Carpenter 1982; Philander 1990; Li 1997; Neelin et al. 1998; see Li and Hsu 2017 for a recent review).

One of important characteristics of ENSO is its interdecadal variability (Trenberth and Shea 1987; Wang 1995; Gu and Philander 1997; Wang and An 2002; Lübbecke and Mcphaden 2014). Gu and Philander (1997) proposed that the ENSO decadal variation lied in the tropical response to extratropical forcing. Wang and An (2002) suggested the ENSO change was rooted in the change of background wind and associated ocean upwelling at the equator Xiang et al. (2013). and Chung and Li (2013) attributed the change of El Niño behavior to interdecadal background mean state change. On one hand, a strengthened cold background SST in the eastern equatorial Pacific around 1999 caused a subsidence in central Pacific, which modulated the El Niño induced anomalous precipitation and wind patterns (Xiang et al. (2013). On the other hand, a sharpened zonal SST gradient across the equatorial Pacific favored the westward

✉ Yuhan Gong
sdgyh1995@163.com

- ¹ Key Laboratory of Meteorological Disaster, Ministry of Education (KLME)/Joint International Research Laboratory of Climate and Environmental Change (ILCEC)/ Collaborative Innovation Center On Forecast and Evaluation of Meteorological Disasters (CIC-FEMD), Nanjing University of Information Science and Technology, Nanjing, China
- ² Department of Atmospheric Sciences, School of Ocean and Earth Science and Technology, International Pacific Research Center, University of Hawaii At Manoa, Honolulu, HI 96822, USA
- ³ State Key Laboratory of Numerical Modeling for Atmospheric Sciences and Geophysical Fluid Dynamics (LASG), Institute of Atmospheric Physics, Chinese Academy of Sciences, Beijing 100029, China
- ⁴ State Key Laboratory of Loess and Quaternary Geology (SKLLQG), Institute of Earth Environment, Chinese Academy of Sciences, Xi'an 710061, China

shifting of anomalous precipitation and wind response to a given SST anomaly (SSTA) (Chung and Li 2013). Lübbecke and McPhaden (2014) pointed out that the ENSO amplitude became weaker after 1999 because colder mean background SST in the eastern equatorial Pacific prevents an effective thermocline feedback.

The change of background SST in other basins may also affect the Pacific (e.g., Solman et al. 2002; Saenko et al. 2004; Luo et al. 2010). The Atlantic Multi-decadal Oscillation (AMO) is characterized by a basin-wide warming or cooling in the Northern Atlantic (Kerr 2000). A positive (negative) AMO phase means a warming (cooling) over most part of North Atlantic. Wang et al. (2014) showed that AMO has a close relation with the Atlantic Meridional Overturning Circulation (AMOC) and the North Pacific SSTA. Equatorial Atlantic SSTA may have a direct impact on ENSO through anomalous large-scale Walker circulation (Jansen et al. 2009; Frauen and Dommenges 2012; Kucharski et al. 2015). It was noted that AMO had a negative correlation with ENSO amplitude (Dong et al. 2006). However, specific processes through which AMO influences ENSO amplitude is unclear to date.

Dong et al. (2006) suggested that AMO may affect ENSO through atmospheric bridge. When AMO is at a warm phase, the Pacific trade wind is reduced, which may

deepen thermocline and reduce the vertical stratification in equatorial Pacific, causing suppressed ENSO amplitude. Kang et al. (2014) proposed that a positive phase of AMO could induce easterly wind stress anomalies in the central equatorial Pacific (CEP) through a Kelvin wave response, causing a cold background mean SST over CEP. This leads to westward shift of ENSO induced zonal wind anomaly, causing more central Pacific (CP)-type El Niños. Yu et al. (2015) suggested that a positive AMO might strengthen the Pacific meridional mode (PMM) and thus the subtropical-tropical coupling, leading to more frequent occurrence of CP-El Niños. With the aid of coupled models, Zanchettin et al. (2016) considered the effect of AMO in modulating the ENSO amplitude through the mean thermocline change in tropical Pacific. Based on the observational analysis and model experiments, Levine et al. (2017) found that the AMO can have a strong influence on the tropical Pacific Ocean by altering the Walker circulation, leading to the distinctive pattern of multi-decadal ENSO variability.

Additionally, the AMO may affect ENSO amplitude via modulating the activity of high-frequency (HF) wind forcing, since the HF wind forcing plays a critical role in triggering ENSO onset or modulating ENSO amplitude (Luther et al. 1983; Kessler et al. 1995; Kerr 2000; Vecchi and Harrison

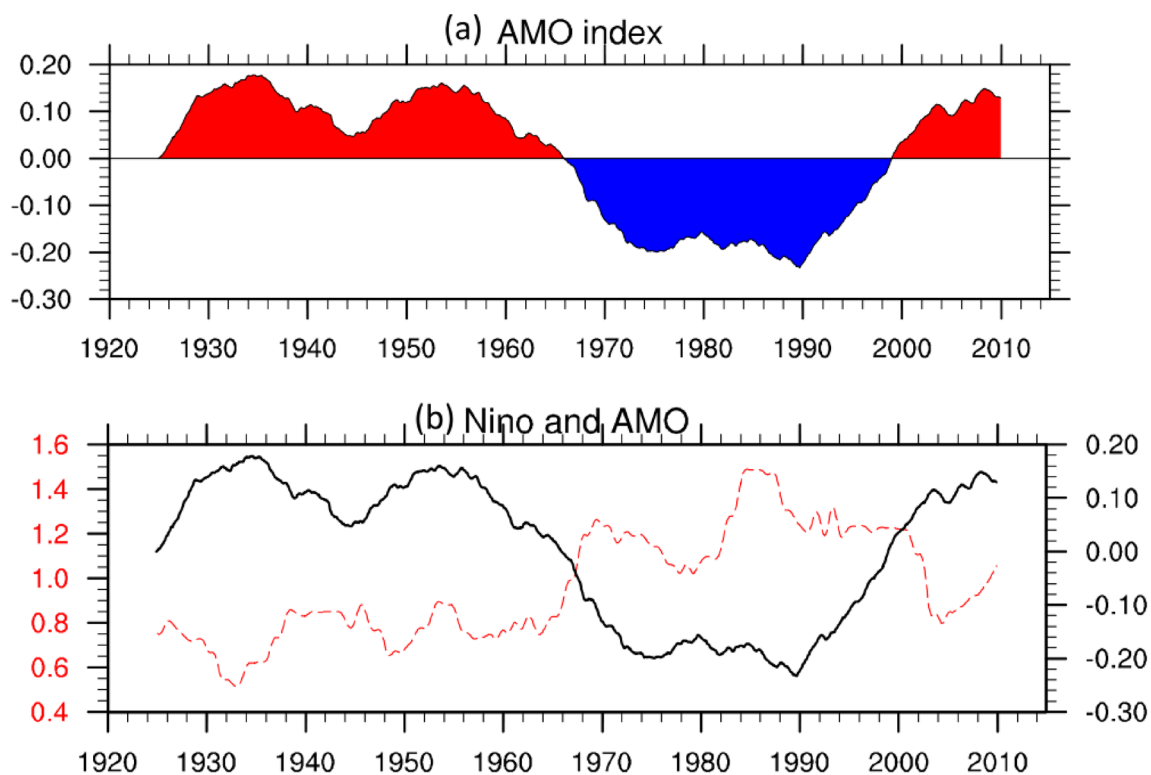


Fig. 1 **a** Time series of 10-year running mean SSTA averaged over North Atlantic (0–60° N, 0–80° W). **b** Time evolution of ENSO amplitude (red) and the AMO index (black) shown in **a**. ENSO

amplitude at each year is defined as the standard deviation of 2–7-year filtered Niño3.4 index in a 13-year window

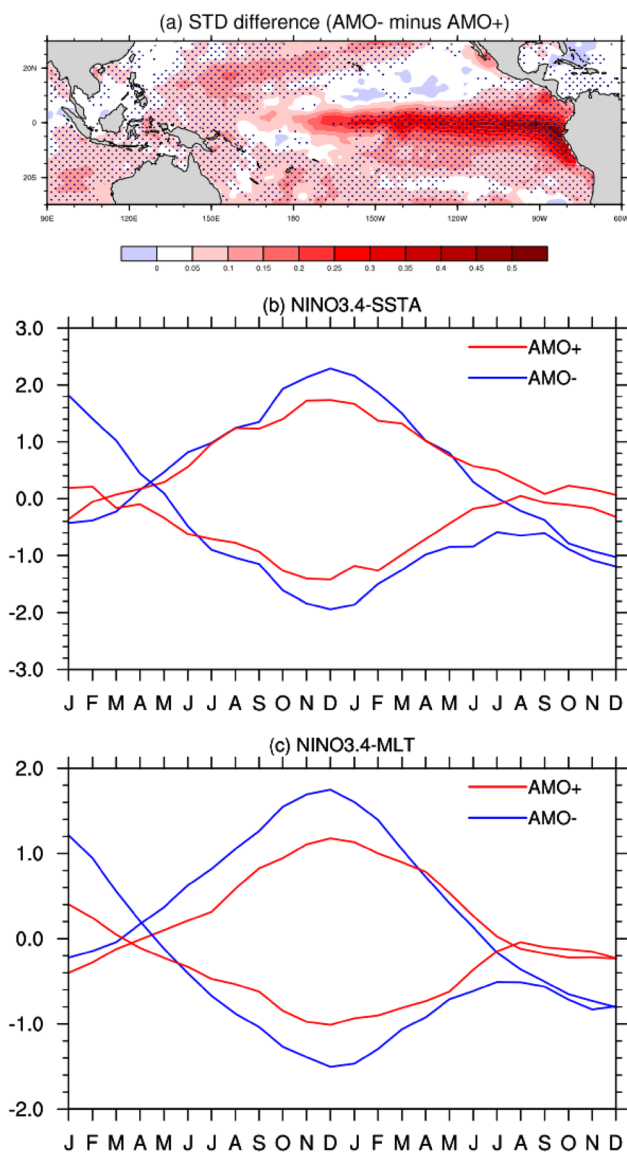


Fig. 2 **a** The difference of SSTA standard deviation between AMO – and AMO+phase. The stippling indicates the difference exceeding 95% confidence level using Student’s t test. Composite time evolutions of **b** SSTA and **c** mixed layer temperature anomaly over the Niño3.4 region (5° N–5° S, 170°–120° W) for El Niño and La Niña during AMO – (blue) and AMO+ (red) phase

2000; Lengaigne et al. 2004; Chen et al. 2016a, 2017a). The HF disturbance may be related to thermodynamic control on deep convection (Hoerling et al. 1997). This process may not be non-linear rectification, however, it also has power at the low-frequency parts and further modulate ENSO variability (e.g. Roulston and Neelin 2000; Levine and Jin 2010). Williamson et al. (2018) found that the collapse of the Atlantic Meridional Circulation (AMOC) which is strongly associated with the AMO could help ENSO eastward shift through decreased stochastic forcing.

Motivated by the aforementioned studies, we intend to conduct a quantitative investigation of the ocean mixed layer heat budget, to understand underlying physical mechanisms behind the observed AMO–ENSO amplitude relationship. Given that ENSO evolution involves a number of positive and negative feedback processes, a special attention will be paid to specific processes that give rise to ENSO tendency difference between positive and negative phases of AMO. The remaining paper is organized as following. In Sect. 2 the data and methods will be described. In Sect. 3 the detailed diagnosis of ENSO structure and evolution and mixed layer heat budget analysis will be carried out. The diagnosis of relative role of the mean state and perturbation changes and various air–sea feedback processes during positive and negative phases of AMO will be conducted and a comprehensive understanding of physical mechanisms through which AMO modulates ENSO amplitude will be given in Sect. 4. Finally a summary and discussion will be given in the last section.

2 Data and methods

Primary data used for the current study include (1) monthly sea surface temperature from HadISST (Rayner et al. 2003) for the period of 1920–2015, (2) monthly ocean temperature, zonal velocity (u), meridional velocity (v), vertical velocity (w) and zonal wind stress (τ_x) from SODA2.2.4 (Carton and Giese 2008) for the period of 1925–2008, (3) monthly surface heat flux from NOAA-20CR (Compo et al. 2011) (4) daily precipitation and wind fields from ERA-20C (Poli et al. 2015) for the period of 1925–2010, and (5) daily specific humidity (q) from ERA-40 (Uppala et al. 2005) for the period of 1958–1979 and from ERA-Interim (Berrisford et al. 2011) for the period of 1979–2010.

To understand the relative role of dynamic and thermodynamic processes in regulating ENSO amplitude during positive and negative AMO phases, the ocean mixed layer heat budget is diagnosed, following Li et al. (2002), Hong et al. (2008) and Chen et al. (2015). The mixed layer temperature anomaly tendency equation may be written as follows:

$$\begin{aligned} \frac{\partial T'}{\partial t} = & - \left(u' \frac{\partial \bar{T}}{\partial x} + \bar{u} \frac{\partial T'}{\partial x} + u' \frac{\partial T'}{\partial x} \right) \\ & - \left(v' \frac{\partial \bar{T}}{\partial y} + \bar{v} \frac{\partial T'}{\partial y} + v' \frac{\partial T'}{\partial y} \right) \\ & - \left(w' \frac{\partial \bar{T}}{\partial z} + \bar{w} \frac{\partial T'}{\partial z} + w' \frac{\partial T'}{\partial z} \right) + \frac{Q'_{net}}{\rho C_p H} + R \end{aligned} \tag{1}$$

The diagnosis of the mixed layer heat budget is confined over the Niño3.4 region (5° S–5° N, 170° W–120° W). In Eq. (1), T denotes the mixed layer temperature, u , v , and w represent three-dimensional (3D) ocean current, $\partial/\partial x$, $\partial/\partial y$,

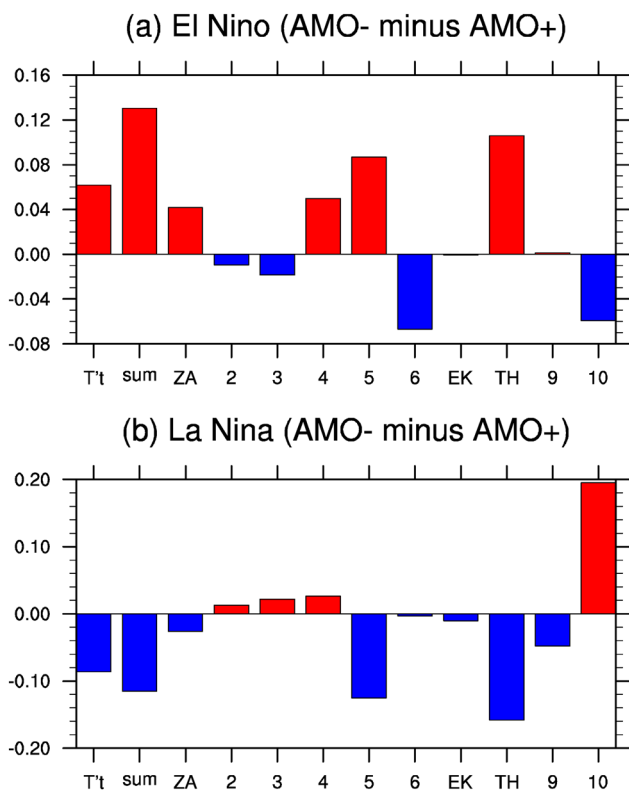


Fig. 3 Composite difference (AMO – minus AMO+ phase) of El Niño and La Niña mixed layer temperature budget terms. $T't$ denotes the change in mixed layer temperature tendency (left hand side of Eq. 1). *sum* is the summation of 10 terms in right hand side of Eq. 1. They are from left to right: $d(-u'\partial\bar{T}'/\partial x)$ (bar 1 denoted by ZA), $d(-\bar{u}\partial T'/\partial x)$ (bar 2), $d(-u'\partial\bar{T}'/\partial x)$ (bar 3), $d(-v'\partial\bar{T}'/\partial y)$ (bar 4), $d(-\bar{v}\partial T'/\partial y)$ (bar 5), $d(-v'\partial T'/\partial y)$ (bar 6), $d(-w'\partial\bar{T}'/\partial z)$ (bar 7 denoted by EK), $d(-\bar{w}\partial T'/\partial z)$ (bar 8 denoted by TH), $d(-w'\partial T'/\partial z)$ (bar 9), $d(Q'_{net}/\rho C_p H)$. Here *d* denotes the difference between negative and positive AMO phase (AMO – minus AMO+ phase)

and $\partial/\partial z$ denote the 3D gradient operator, a prime represents the interannual anomaly, a bar denotes the climatological mean state, and the first nine terms on the right-hand side of the equation are 3D temperature advection terms. Q_{net}



Fig. 4 Relative contributions (unit: K month⁻¹) of the mean state change and the perturbation change to the Bjerknes thermocline feedback term ($-\bar{w}\partial T'/\partial z$) and the zonal advective feedback term ($-u'\partial\bar{T}'/\partial x$). For each term, four columns represent $d(A'B)$, $d(A')B$, $A'd(B)$, $d(A')d(B)$, respectively.

denotes the net surface heat flux term that includes surface shortwave and longwave radiation and latent and sensible heat fluxes (with a positive sign representing that the ocean receives heat), R denotes the residual term, ρ is the density of water ($=10^3 \text{ kg m}^{-3}$), C_p is the specific heat of water ($=4000 \text{ J kg}^{-1} \text{ K}^{-1}$), and H denotes the mixed layer depth. The mixed layer depth is defined as a depth where oceanic temperature is $0.5 \text{ }^\circ\text{C}$ below the surface temperature.

Following Chen et al. (2015), we use a Z test (Bluman 2007) to examine the statistical significance. Z has the following formula:

$$Z = \frac{Z_{r_1} - Z_{r_2}}{\sqrt{\frac{1}{n_1-3} + \frac{1}{n_2-3}}} \quad (2)$$

where Z_r is the Fisher transfer,

$$Z_r = \ln \sqrt{\frac{1+r}{1-r}} \quad (3)$$

and r_1 (r_2) and n_1 (n_2) represent the wind stress–thermocline correlation coefficients and the sample number for AMO negative (positive) phase. According to the equations above, for current sample size, the region where the absolute value of Z exceeds 1.96 means that it is statistically significant (i.e., exceeding a 95% confidence level).

3 Observed relationship between ENSO intensity and AMO

Figure 1a shows the time series of the AMO index, which is defined as a 10-year running mean of SSTA averaged in the North Atlantic ($0\text{--}60^\circ \text{ N}$, $0\text{--}80^\circ \text{ W}$), following Dong et al. (2006). The SST data has been detrended before the index was calculated, to remove the effect of global warming.

According to the AMO time series, we selected 1925–1965 and 1999–2010 as AMO+ phase and 1966–1998 as AMO – phase. El Niño and La Niña events were selected

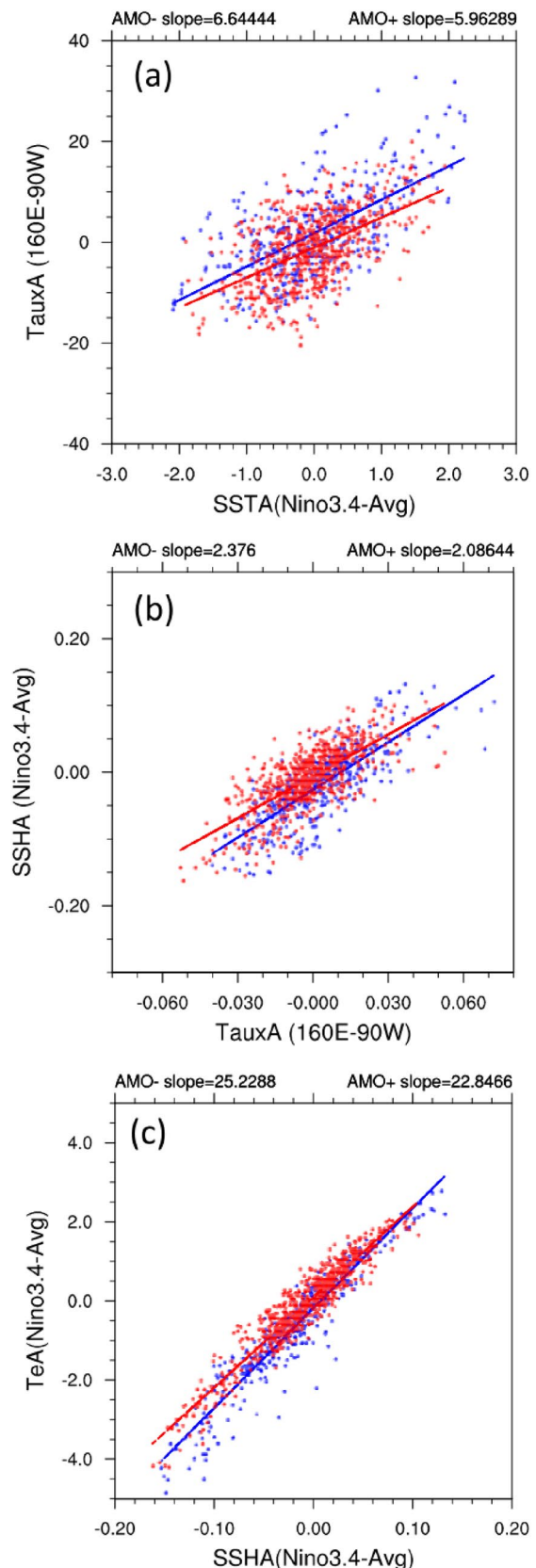
$A'd(B)$ and $d(A')d(B)$, respectively. Here $d()$ denotes the difference between AMO cold and warm phase (cold minus warm), A' denotes the perturbation variable, and B denotes the basic state variable

Fig. 5 Scatter diagrams of **a** area-averaged τ'_x over 160°E – 90°W , 5°S – 5°N (10^{-3}Nm^{-2}) versus Niño-3.4 SSTA ($^\circ\text{C}$), **b** Niño-3.4 SSH anomaly (m) versus the area-averaged τ'_x (10^{-3}Nm^{-2}) and **c** Niño-3.4 subsurface temperature T'_e ($^\circ\text{C}$) versus Niño-3.4 SSH anomaly (m) during AMO – (blue dots and slope) and AMO+ (red dots and slope) phase

based on the criterion that the SSTA and mixed layer temperature anomaly (MLTA) averaged over the Niño3.4-region (5°N – 5°S , 170° – 120°W) in DJF exceed positive and negative one standard deviation. The so selected El Niño events are in 1925, 1930, 1940, 1951, 1957, 1965, 1972, 1982, 1986, 1991, 1994, 1997 and 2006, and so selected La Niña events are in 1938, 1942, 1949, 1955, 1961, 1964, 1970, 1973, 1983, 1988, 1995, 1998 and 2007. To examine the time evolution of ENSO amplitude, we define ENSO amplitude at a given year as the standard deviation of Niño3.4 SSTA in a 13-year window. Figure 1b shows the time evolution of ENSO amplitude and the AMO index. Note that ENSO intensity coincides well with the phase of the AMO, and their temporal correlation coefficient is -0.85 . When the AMO is in a negative (positive) phase, the ENSO amplitude is stronger (weaker). This result is consistent with previous studies with a shorter analysis period (e.g., Dong et al. 2006; Kang et al. 2014; Yu et al. 2015).

To verify the result above, we further calculated the standard deviation of the interannual SSTA in the tropical Pacific during AMO – and AMO+ phases. Figure 2a shows the difference of the standard deviation between the two phases (negative phase minus positive phase). Obviously, the ENSO standard deviation in AMO negative phase is larger, consistent with Fig. 1b. The region with the largest difference (greater than 0.5°C) lies in the eastern equatorial Pacific (EEP). Therefore, during AMO negative phase SSTA in EEP is stronger and the ENSO magnitude is stronger.

Next we examine the ENSO evolution difference. The composite time evolutions of SSTA and MLTA averaged in Niño3.4-region are shown in Fig. 2b, c. It is clearly seen that both El Niño and La Niña develop quickly and peak in northern winter during both the AMO positive and negative phases. The amplitude of both El Niño and La Niña is greater during AMO – phase. As a result, the growth rate of both El Niño and La Niña is greater during AMO – phase than AMO+ phase. In the following we will diagnose the MLTA tendency to understand the fundamental cause of ENSO amplitude modulation between AMO positive and negative phase.



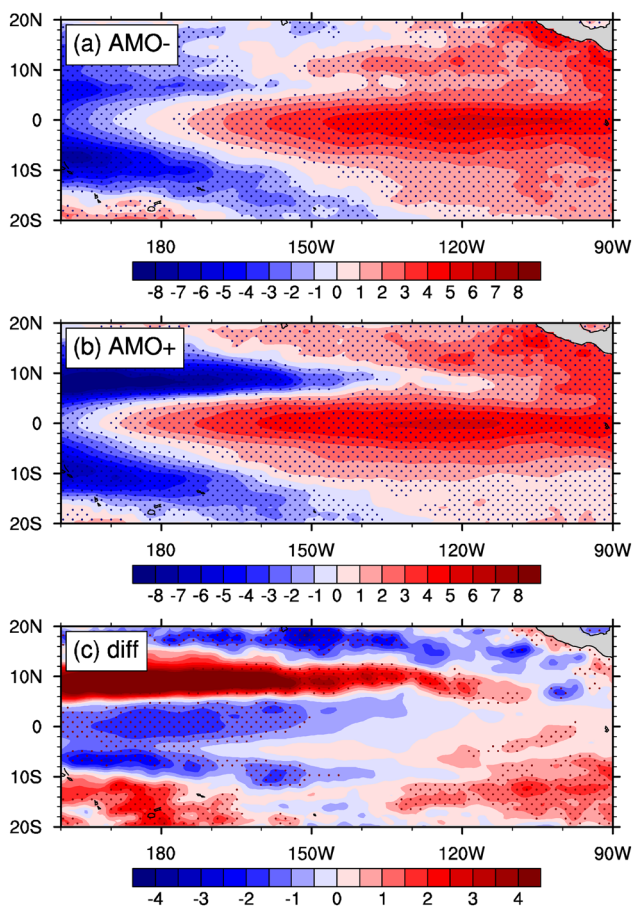


Fig. 6 SSH anomaly fields regressed onto the area-averaged τ'_x over $5^\circ \text{ S}–5^\circ \text{ N}$, $160^\circ \text{ E}–90^\circ \text{ W}$. Units: $[\text{m} (\text{N m}^{-2})]$. The stippling in **a**, **b** indicates the regression coefficient exceeding 95% confidence level using Student's *t* test. The stippling in **c** indicates the changes in the regressions coefficients exceeding 95% confidence level using a *Z* test

4 Mechanisms for AMO modulation on ENSO amplitude

To understand the relative roles of oceanic dynamics and thermodynamic terms in contributing to ENSO amplitude difference, we conduct a mixed layer heat budget analysis over EEP. Our diagnosis is focused on ENSO developing phase. According to Fig. 2c, El Niño developing phase is from May to November, whereas La Niña developing phase is from July to December.

Figure 3 shows the difference of each of the budget terms between AMO – and AMO + phase for composite El Niño and La Niña respectively. A positive (negative) MLTA tendency sign for El Niño (La Niña) implies that both El Niño and La Niña tendencies are greater during AMO – phase than during AMO + phase. Comparing both El Niño and La Niña cases, one may find the greatest common term is attributed to Bjerknes thermocline

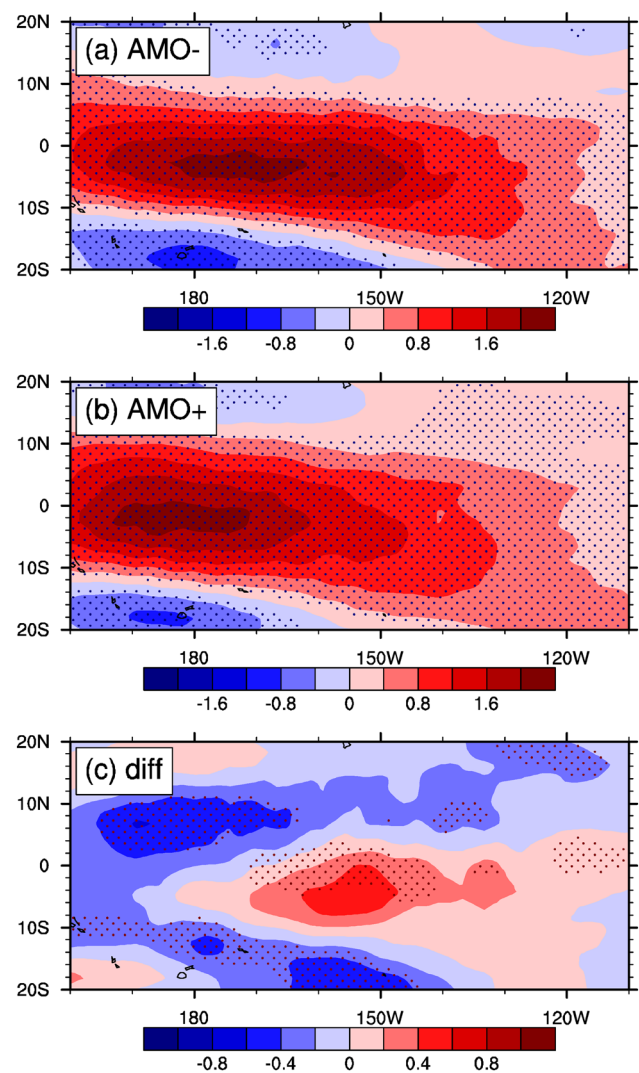
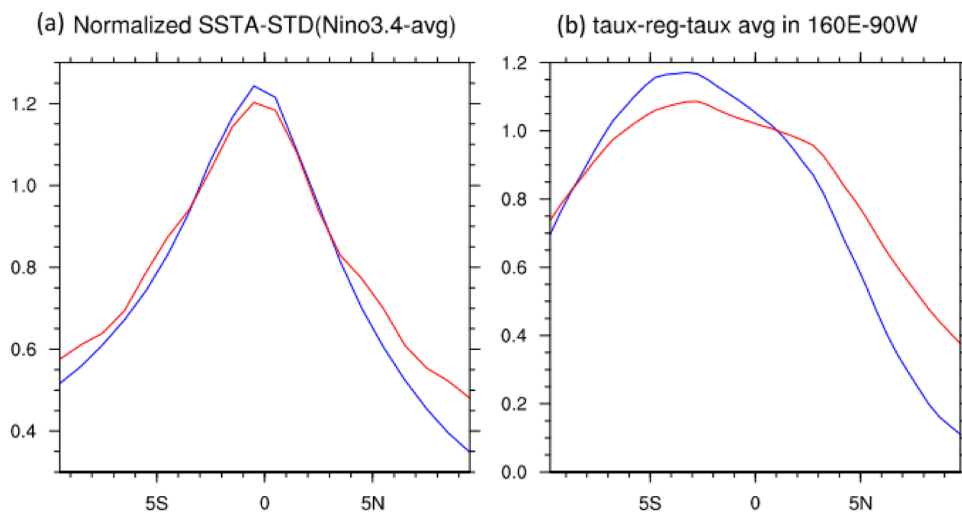


Fig. 7 Same as Fig. 6 except for τ'_x field. Units: $[(\text{N m}^{-2}) (\text{N m}^{-2})]$. The stippling in **a**, **b** indicates the regression coefficient exceeding 95% confidence level using Student's *t* test. The stippling in **c** indicates the changes in the regressions coefficients exceeding 95% confidence level using a *Z* test

feedback term (i.e., term 8 $-\bar{w}\partial T'/\partial z$), followed by meridional advective feedback term (term 5) and zonal advective feedback term (term 1, $-u'\partial \bar{T}/\partial x$). As shown in previous studies (e.g., Chen et al. 2016b, 2017b), meridional advective feedback is simply a amplifier, and its effect depends on the net effect of other feedback processes. Thus in the following we will focus on examining the Bjerknes thermocline feedback and the zonal advective feedback terms.

Note that each of the feedback terms above is the product of the mean and anomaly field. Therefore it is desirable to understand their relative contribution. Following Chen et al. (2015), we separate their relative contributions based on the following equation:

Fig. 8 Meridional profiles of (a) normalized SSTA standard deviation field (i.e., divided by the SSTA magnitude over Niño-3.4) and (b) meridional profiles of zonal mean τ'_x regressed onto the area-averaged τ'_x time series over 160° E–90° W, 5° S–5° N during AMO – (blue) and AMO + (red) phase



$$\Delta(A'B) = \Delta(A')B + A\Delta(B) + \Delta(A')\Delta(B), \tag{4}$$

where $\Delta(\)$ denotes the difference of the AMO negative and positive phase, A' represents the perturbation field and B represents the mean state field. Thus the difference of a product can be separate to three parts: the difference due to the perturbation change, the difference due to the mean state change, and the difference due to covariance of the mean state and perturbation changes.

Figure 4 depicts the relative roles of the perturbation and mean state change for the thermocline feedback and zonal advective feedback terms. The major contributor lies in the perturbation change in both the feedback terms. Thus, the result indicates that the mean state change between AMO – and AMO + phase is not critical for the distinctive thermocline and zonal advective feedbacks. It is the change of ENSO perturbation part between the two AMO phases that eventually causes the mixed layer heat budget difference.

The growth rate associated with the Bjerknes thermocline feedback ($-\bar{w}\partial T'/\partial z$) can be written as (Liu et al. 2011; Chen et al. 2015, 2017b):

$$\sigma = \frac{\bar{w}}{H}R(\tau'_x, T')R(D', \tau'_x)R(T'_e, D'), \tag{5}$$

where \bar{w} is the mean vertical velocity, τ'_x is the zonal wind stress anomaly, D' is the thermocline depth anomaly, and T'_e is the subsurface ocean temperature anomaly. Equation (5) states that the strength of the thermocline feedback depends on three air–sea interaction processes on the interannual time scale. $R(\tau'_x, T')$ represents how strong atmospheric zonal wind stress (τ'_x) in basin equatorial Pacific responds to unit SSTA forcing in EEP. $R(D', \tau'_x)$ denotes how ocean thermocline in EEP responds to unit zonal wind stress (τ'_x) forcing in basin equatorial Pacific. $R(T'_e, D')$ represents how ocean subsurface temperature responds to unit thermocline depth change in EEP.

To quantify each of the air–sea interaction processes, we draw scatter diagrams and use the slopes to represent the responses during AMO – and AMO + phases respectively. Figure 5 shows that all three slopes (or responses) are larger in AMO – phase. This indicates that the three processes are all important in contributing to the different Bjerknes thermocline feedbacks between AMO negative and positive phases. The rates of the slope changes for the three processes are 12.7%, 13.2% and 10.4% respectively.

In the following we discuss the effect of AMO on these slope changes. Because $R(D', \tau'_x)$ has the largest percentage change, we first examine this feedback process. It reflects the ocean thermocline response in EEP to unit zonal wind stress (τ'_x) forcing in basin equatorial Pacific. In response to a positive zonal wind stress anomaly, thermocline depth (D') exhibits a tilting response. Letting sea surface height (SSH) anomaly as a proxy of D' , one may regress SSH' onto equatorial τ'_x (Fig. 6). Here we employed the effective degree of freedom proposed by Bretherton et al. (1999) when conducting the t-test for the regression results as displayed in Figs. 6a, b and 7a, b. The specific effective degree of freedom is given below:

$$N_E = N \frac{1 - Cor_1 Cor_2}{1 + Cor_1 Cor_2} \tag{6}$$

where N_E denotes the effective degree of freedom, N is the original length of time series, Cor_1 (Cor_2) denotes the lag – 1 autocorrelation of the first (second) variable. As shown in Fig. 6, the thermocline tilting in response to unit wind stress forcing is greater during AMO – phase.

The cause of this distinctive thermocline response is attributed to the meridional structure of τ'_x , as discussed by Chen et al. (2015, 2017b). A narrower meridional structure implies greater amplitude at the equator. To clearly illustrate this meridional structure change, we plotted regressed

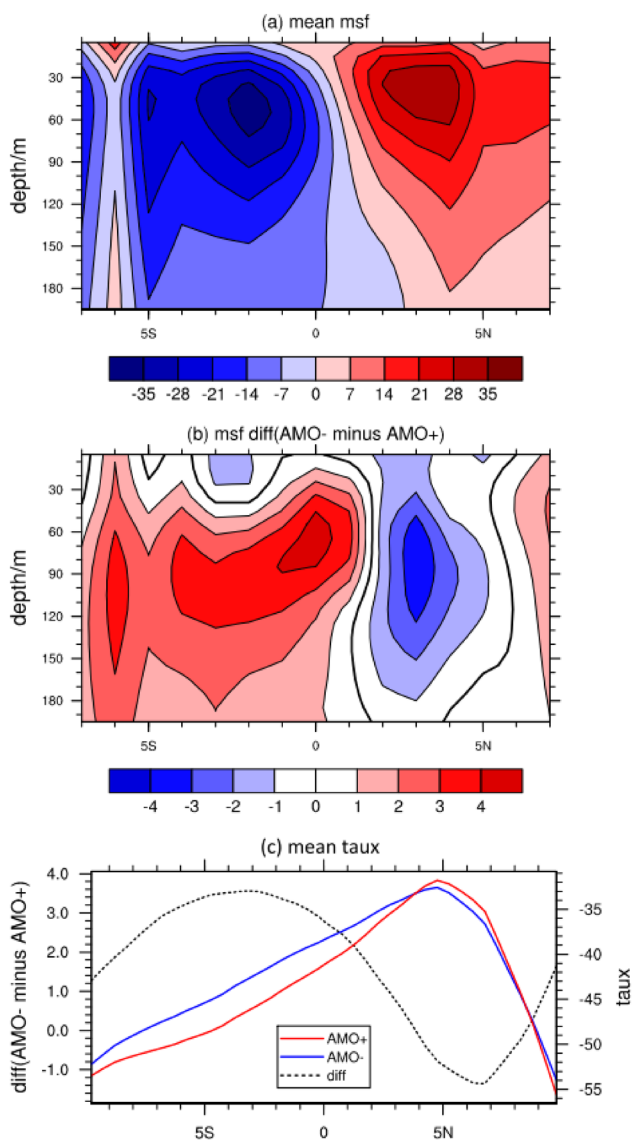


Fig. 9 **a** Climatological zonal mean meridional stream function in the Pacific, **b** the difference of zonal mean meridional stream function between AMO – and AMO+ phase, and **c** meridional profiles of τ_x averaged over 160° E–90° W during AMO – (blue) and AMO+ (red) phase and their difference (AMO – minus AMO+ phase, dashed black curve). Right y-axis in **c** is for total τ_x and left y-axis is for their difference

τ'_x field for AMO – and AMO+ phases and their difference (Fig. 7). Indeed, as shown in the difference map (AMO – minus AMO+ phase) (Fig. 7c), a larger zonal mean τ'_x appears at the equator, and a smaller τ'_x appears in the off-equatorial region. As a result, the meridional width of τ'_x becomes narrower (wider) during AMO – (AMO+) phase.

The change of meridional structure of τ'_x during the different AMO phases is consistent with the change of the SSTA structure, as shown in Fig. 8. Such a consistent change is physically reasonable, because the wind and SSTA anomalies

associated with ENSO are tightly coupled. During AMO – phase, the SSTA meridional width is narrower, and so is τ'_x (Fig. 8).

What controls the meridional structure of the ENSO perturbation? According to Chen et al. (2015, 2017b), it is controlled primarily by the strength of the mean subtropical cell (STC). Figure 9a illustrates the vertical-meridional distributions of climatological zonal mean meridional stream function in the Pacific. It is characterized by an upwelling near the equator, a downwelling in the off-equatorial region, and poleward flows near the surface. The difference map (i.e., AMO – minus AMO+ phase, Fig. 9b) shows an opposite anomalous meridional stream function field, indicating that the STC anomaly is against the climatological STC during the negative AMO phase. Thus, the STC is weaker in AMO – phase, leading to narrower SSTA and τ'_x patterns.

A further examination shows that the weaker STC during AMO – phase is attributed to the weakening of the trade wind in the tropics. As shown in Fig. 9c, mean trade wind stress is weaker in most of tropics during AMO – phase. A weakened trade reduces the strength of STC.

Next we examine the feedback parameter $R(\tau'_x, T')$. This parameter measures how strong the atmospheric convection and wind respond to unit SSTA forcing in EEP. Figure 10 shows composite precipitation and 850 hPa wind anomaly patterns. Both the precipitation and wind anomalies are stronger during AMO – phase than during AMO+ phase. A similar difference pattern is found when the wind and precipitation anomaly fields are normalized by the Nino3.4 SSTA. It follows that the precipitation and wind response to the EEP SSTA is larger during AMO – phase. The enhanced wind stress anomaly promotes a stronger thermocline and zonal surface oceanic current response, leading to a stronger Bjerknes thermocline feedback and zonal advective feedback.

Why is the atmospheric response to SSTA different between AMO – and AMO+ phase? It is noted that low-level specific humidity is larger during AMO – phase (Fig. 11a), so that the same anomalous convergence or ascending motion could lead to a stronger precipitation and thus wind response. But what causes the increase of the specific humidity in AMO – phase in the first place? Figure 11b illustrates the SST and 850 hPa wind difference patterns between the two AMO phases. There is a weak warming in EEP and cooling in mid-latitude Pacific. Along the equator from Indian Ocean to central Pacific, there is pronounced westerly wind anomaly. It is likely that this westerly is a response to the negative heating in the tropical Atlantic associated with AMO – phase. The cold SSTA in tropical Atlantic may induce a Kelvin wave response to the east, as shown by Rong et al. (2010), Li et al. (2016) and Yu et al. (2016). Some previous studies put forward another possible mechanism to explain the mean surface zonal wind change

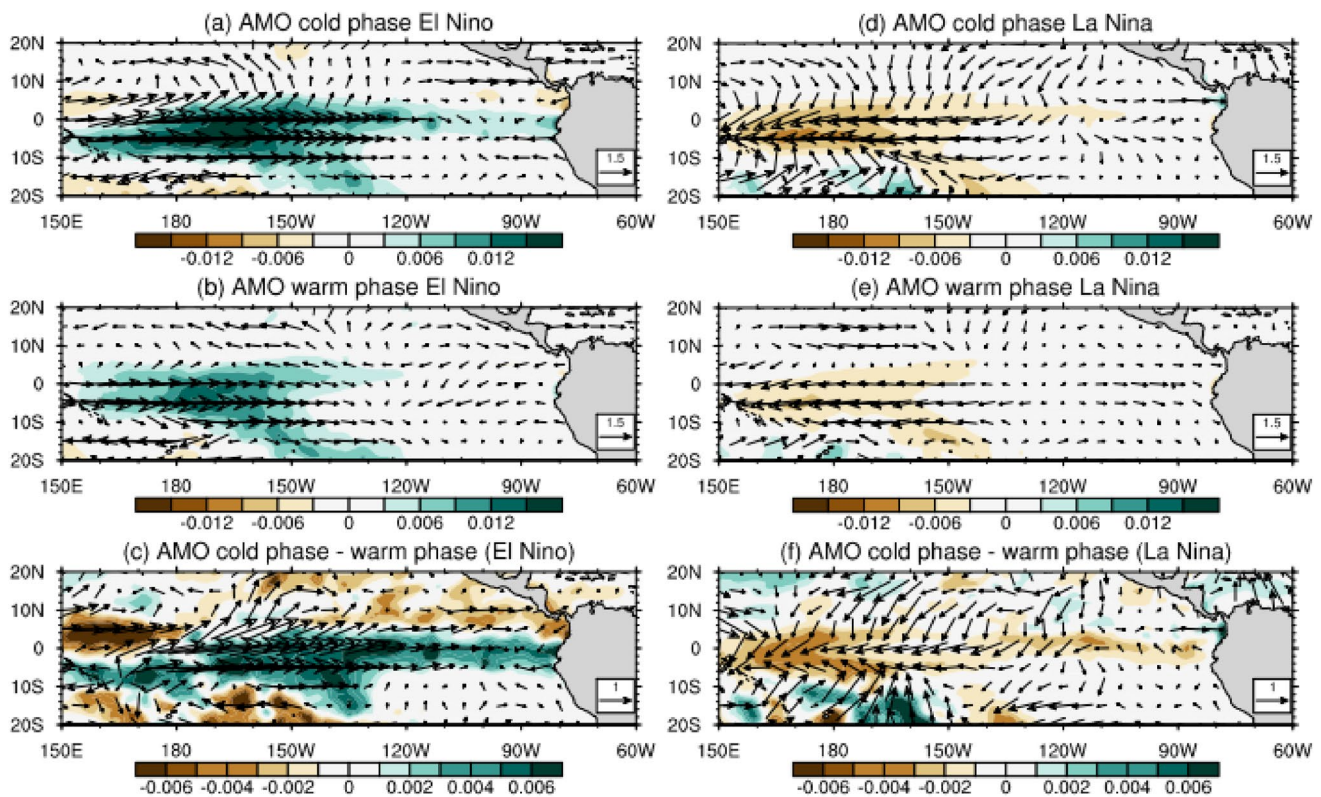


Fig. 10 Composite anomalous precipitation (shading; kg m^{-2}) and 850 hPa wind (vectors; m/s) fields for El Niño (left) and La Niña (right) during AMO – phase (top), AMO+phase (middle) and their difference (AMO – minus AMO+phase, bottom)

in tropical Pacific. The cold SSTa in tropical Atlantic could weaken the Walker circulation in the tropical Pacific, leading to the decrease of trade wind in the central equatorial Pacific and the resultant westerly wind anomaly in the tropical Pacific (Mcgregor et al. 2014; Li et al. 2016; Levine et al. 2018). The westerly anomaly may transport high mean moisture from the warm pool eastward, causing the increase of low-level specific humidity in the equatorial Pacific.

Thirdly, we examine the feedback parameter $R(T'_e, D')$. As stated previously, this parameter measures how strong the ocean subsurface temperature responds to unit thermocline depth change. It is noted that the background mean vertical temperature gradient ($\partial \bar{T} / \partial z$) is greater during AMO – phase compared to AMO+phase (Fig. 12). Thus, given the same thermocline perturbation, the change of subsurface temperature is greater during AMO – phase. This explains why $R(T'_e, D')$ slope is greater in AMO – phase. The background mean temperature gradient increase is partially caused by the weak surface warming in EEP in association with the negative AMO phase.

To sum up, the aforementioned three air–sea interaction processes all contribute to the enhanced Bjerknes thermocline feedback during AMO – phase. In addition, stronger zonal wind and thermocline responses also favor an enhanced zonal advective feedback, because ocean surface

current associated with ENSO is largely determined by geostrophic current anomaly. The enhanced thermocline and zonal advective feedbacks can further strengthen the meridional advective feedback as it depends on the strength of the SSTA at the equator.

A background easterly vertical shear anomaly during AMO – phase may favor the development of high-frequency wind disturbances (Li 2006; Sooraj et al. 2009), which may further strengthen ENSO amplitude through nonlinear rectification (Rong et al. 2011; Chen et al. 2017a). Figure 13 illustrates the difference of background vertical shear and high-frequency (10–90-day filtered) wind variability between AMO – and AMO+phase. Regardless of inclusion of El Niño years or not, high-frequency wind variability is greatly strengthened, particularly over CEP, in association with enhanced easterly vertical shear during the negative AMO phase. While this implies a possible linkage between the high-frequency wind activity and the multi-decadal ENSO modulation, a further in-depth study is needed to understand the physical linkage.

Fig. 11 **a** The difference of 1000–700 hPa averaged specific humidity (g/kg) between AMO – phase and AMO + phase. The stippling indicates the difference exceeding a 95% confidence level using Student’s t test. **b** Difference of mean SST (shading; °C) and 850 hPa wind (vector; m/s) fields between AMO – and AMO + phase

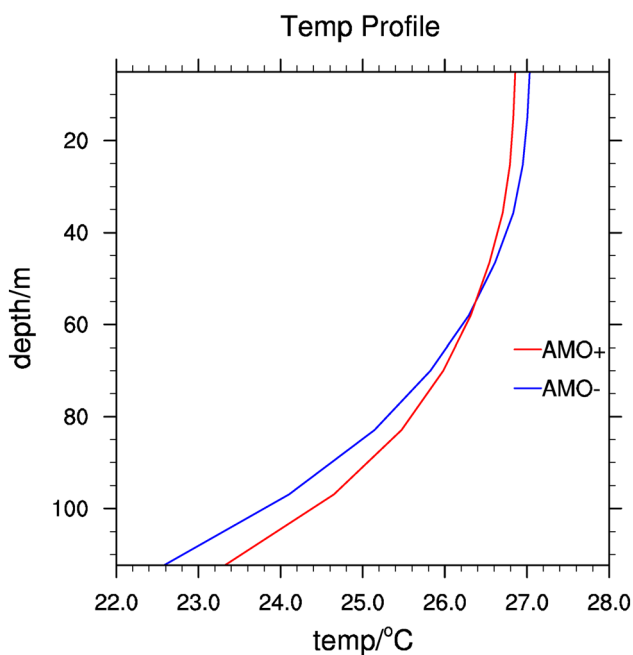
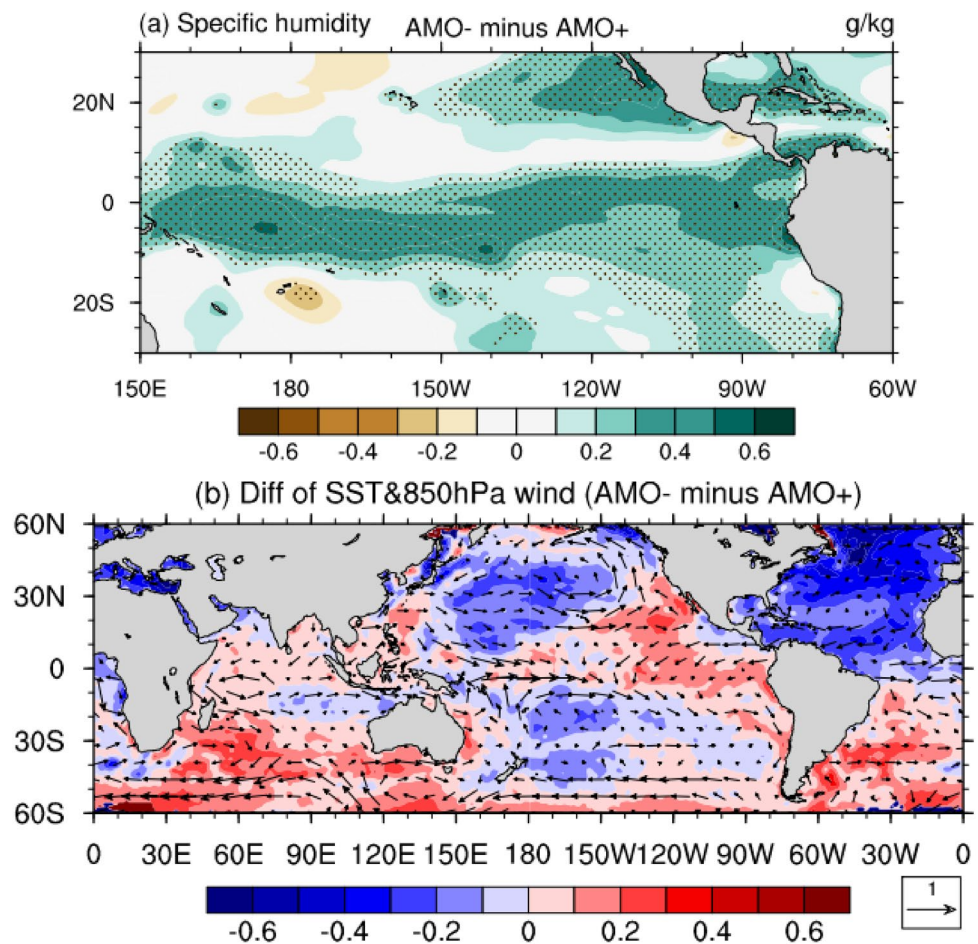


Fig. 12 Background vertical temperature profiles averaged over eastern equatorial Pacific (2° S–2° N, 170° W–120° W) during AMO – (blue) and AMO + (red) phase

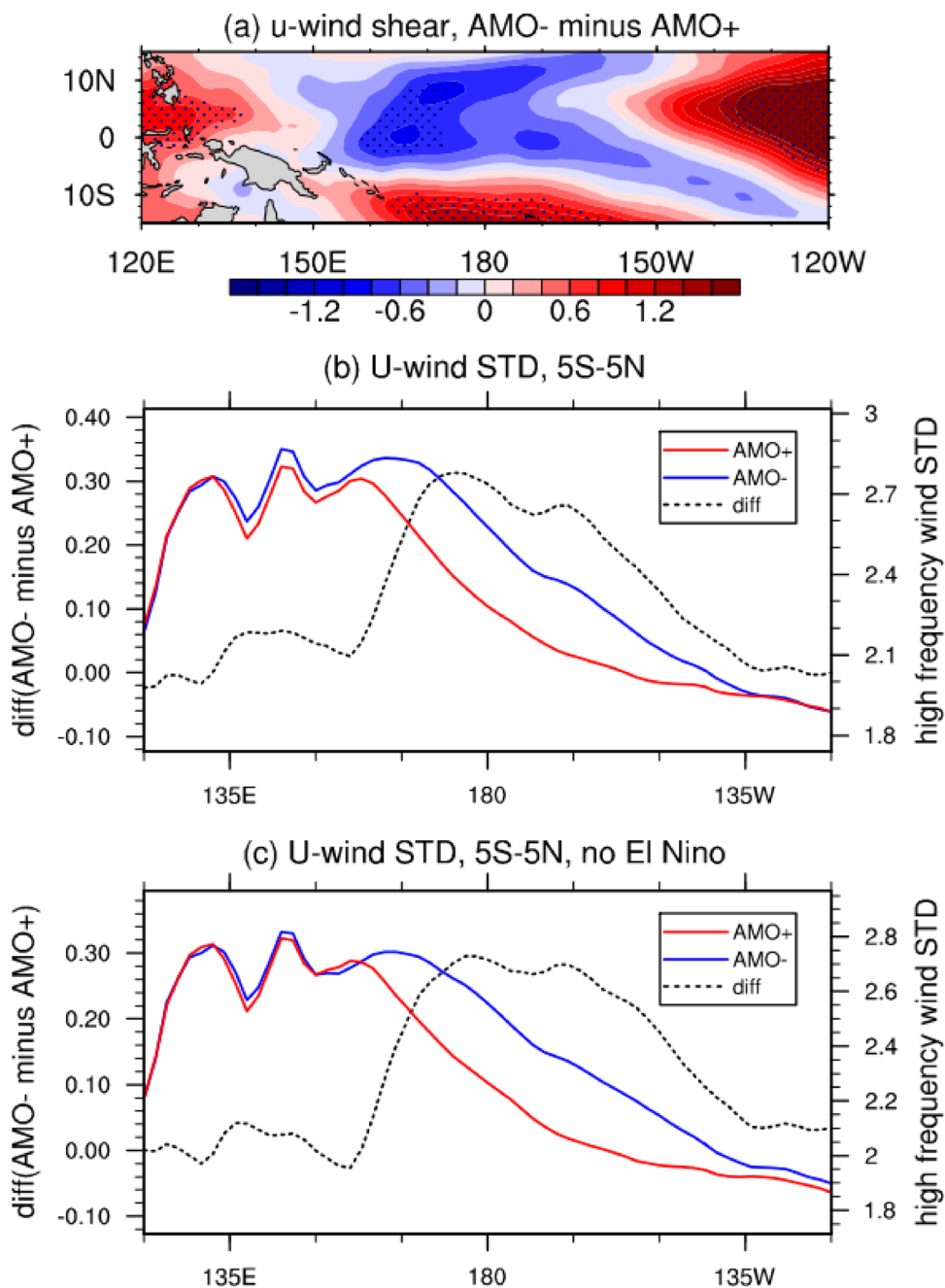
5 Summary and discussion

The effect of AMO on modulating the ENSO amplitude was investigated based on an ocean mixed layer heat budget analysis. It is found that ENSO amplitude and its associated SSTa tendency during the developing phase are negatively correlated to the AMO, that is, ENSO and SSTa tendency are stronger when AMO is in a negative phase, and vice versa. Among various air–sea feedback processes, the Bjerknes thermocline feedback is most important in determining the AMO – ENSO amplitude relation.

The relative role of the mean state and perturbation change in affecting the air–sea feedback processes is further examined. It is found that the perturbation change is critical. Thus the mean state change does not affect the feedback directly but through its impact on the perturbation structure.

Specific mechanisms through which AMO affects ENSO intensity are described as following. During the negative AMO phase, the cold SSTa in tropical Atlantic induced anomalous westerly over equatorial Indian Ocean and western Pacific. The westerly anomaly advected high mean moisture eastward, increasing moisture in the equatorial Pacific. As a result, atmospheric precipitation and wind responses

Fig. 13 **a** Difference of background vertical shear of zonal wind ($u_{200}-u_{850}$) between AMO - and AMO + phase. **b** Standard deviation of 10–90-day band-pass filtered 850 hPa zonal wind average over 5° S– 5° N during AMO - (blue) and AMO + (red) phase. Dashed curve shows the difference (AMO - minus AMO +). Right y-axis is for the wind standard deviation and left y-axis is for the difference. **c** Same as **b** except that El Niño years are removed



to ENSO were enhanced. The reduction of trade wind in the tropical Pacific also caused the weakening of the mean STC, which reduced the meridional width of ENSO perturbation. The narrower meridional structure of ENSO led to an enhanced zonal wind stress anomaly at the equator, favoring a stronger thermocline response to unit wind stress forcing. A larger mean vertical temperature gradient ($\partial\bar{T}/\partial z$) during the negative AMO phase caused a greater subsurface temperature response to unit thermocline depth anomaly. All these processes mentioned above led to a stronger Bjerknes thermocline feedback. In addition, the processes above also

induced stronger zonal and meridional advective feedbacks during the negative AMO phase.

While the current analysis suggested a possible role of high-frequency wind activity associates with the AMO phase in modulating the ENSO amplitude, further observational and modeling studies are required to understand the impact of the AMO on high-frequency eddies and the feedback of the high-frequency variability on the ENSO. One hypothesis for observed multi-decadal ENSO variability is that there are not underlying changes to the stability of the ENSO, but rather that the forcing from high frequency winds

has been randomly greater (e.g., Wittenberg 2009). Another hypothesis is that there are changes to the high frequency forcing that are forced by changes in the AMO that could be constructive or destructive to the change in ENSO signal (e.g., Williamson et al. 2018). A further in-depth study is needed to understand this issue.

A long (say, about 100 years) 3-dimensional dataset is needed to investigate the ENSO amplitude modulation by the AMO, but currently such datasets are quite limited. Thus, the current study mainly used the ocean reanalysis data from SODA2.2.4 and the atmosphere reanalysis product from NOAA-20c and ERA-20c. However, it is interesting to notice that a previous study by Lubbecke and McPhaden (2014) used several ocean reanalysis datasets to calculate the BJ index, in order to investigate the primary difference in the feedback terms between two periods, i.e., 1980–1999 (P1) and 2000–2010 (P2), which coincidentally belongs to an AMO negative phase and an AMO positive phase, respectively. They found that the changes of thermocline feedback and zonal advective feedback are the most dominant terms determining the ENSO variability change in P1 and P2, which is consistent with our diagnosed results. Some recent studies (Chen et al. 2019a, b) also pointed out that the diagnosed results based on the two different diagnostic methods, i.e., BJ index and the mixed layer heat budget analysis, are consistent with each other. Therefore, our diagnosed results building on a single ocean reanalysis are credible, and it is meaningful to check the existing mechanism for AMO–ENSO relationship if we may obtain some other observational or even the modeling datasets covering a long time span in the future.

It is worth mentioning that some recent studies provided an alternative interpretation for the linkage between the AMO and ENSO variability change. Levine et al. (2018) suggested that the SSTa in the tropical North Atlantic during the positive AMO phase could induce enhanced cross-equatorial wind in eastern tropical Pacific, and such a mean state change in the tropical Pacific might play a role in weakening the ENSO amplitude (Hu and Fedorov 2018).

In this study, through the diagnosis of oceanic mixed layer heat budget, we reveal the role of the background mean state change associated with AMO in affecting ENSO air–sea feedback processes. But specific processes through which AMO affects the Pacific mean state are still unclear. In the current study we proposed a direct tropical Kelvin wave response mechanism. It is possible that AMO may affect the Pacific through mid-latitude processes, such as the teleconnection mechanism suggested by Zhang and Delworth (2007) between the Atlantic and North Pacific storm track. Timmermann et al. (2007) proposed that a weakening of the Atlantic Meridional Overturning Circulation might influence ENSO strength through its impact on eastern Pacific mean

state. Further studies are needed to resolve this important issue.

Acknowledgements This work was jointly supported by NSFC Grants 41630423, National Key Research and Development Program on Monitoring, Early Warning and Prevention of Major Natural Disaster (2018YFC1506002), NOAA NA18OAR4310298, and NSF AGS-2006553, the Natural Science Foundation of Jiangsu Province (No. BK20190781), the LASG Open Project, and the Open Fund of State Key Laboratory of Loess and Quaternary Geology (SKLLQG1802). This is SOEST contribution number 11108, IPRC contribution number 1462 and ESMC number 319.

References

- Barnston AG, Livezey RE (1987) Classification, seasonality and persistence of low-frequency circulation patterns. *Mon Weather Rev* 115:1083–1126
- Berrisford P, Dee D, Poli P et al (2011) The ERA-Interim archive version 2.0. Technical Report, ERA Report Series 1, ECMWF, Shinfield Park, Reading UK.
- Bluman AG (2007) Elementary statistics. McGraw-Hill 783 pp.
- Bretherton CS, Widmann M, Dymnikov VP et al (1999) The effective number of spatial degrees of freedom of a time-varying field. *J Clim* 12:1990–2009
- Carton JA, Giese BS (2008) A reanalysis of ocean climate using Simple Ocean Data Assimilation (SODA). *Mon Weather Rev* 136:2999–3017
- Chen L, Li T, Yu Y (2015) Causes of Strengthening and Weakening of ENSO Amplitude under Global Warming in Four CMIP5 Models. *J Clim* 28:3250–3274
- Chen L, Yu Y, Zheng W (2016a) Improved ENSO simulation from climate system model FGOALS-g1.0 to FGOALS-g2. *Clim Dyn* 47:2617–2634. <https://doi.org/10.1007/s00382-016-2988-8>
- Chen L, Li T, Behera SK, Doi T (2016b) Distinctive precursory air–sea signals between regular and super El Niños. *Adv Atmos Sci* 33:996–1004
- Chen L, Li T, Wang B, Wang L (2017a) Formation mechanism for 2015/16 super El Niño. *Sci Rep* 7:2975
- Chen L, Li T, Yu Y, Behera SK (2017b) A possible explanation for the divergent projection of ENSO amplitude change under global warming. *Clim Dyn* 49:3799–3811
- Chen M, Li T, Shen X, Wu B (2016c) Relative roles of dynamic and thermodynamic processes in causing evolution asymmetry between El Niño and La Niña. *J Clim* 29:2201–2220
- Chen L, Zheng W, Braconnot P (2019a) Towards understanding the suppressed ENSO activity during mid-Holocene in PMIP2 and PMIP3 simulations. *Clim Dyn* 1:1095–1110. <https://doi.org/10.1007/s00382-019-04637-z>
- Chen L, Wang L, Li T, Liu J (2019b) Drivers of reduced ENSO variability in mid-Holocene in a coupled model. *Clim Dyn* 52:5999–6014. <https://doi.org/10.1007/s00382-018-4496-5>
- Chung P-H, Li T (2013) Interdecadal relationship between the mean state and El Niño types. *J Clim* 26:361–379
- Compo GP, Whitaker JS, Sardeshmukh PD et al (2011) The twentieth century reanalysis project. *Q J R Meteorol Soc* 137(654):1–28
- Dong B, Sutton RT, Scaife AA (2006) Multidecadal modulation of El Niño–Southern Oscillation (ENSO) variance by Atlantic Ocean sea surface temperatures. *Geophys Res Lett* 33:1
- Dong B, Sutton RT (2007) Enhancement of ENSO variability by a weakened Atlantic thermohaline circulation in a coupled GCM. *J Clim* 20:4920–4939

- Frauen C, Dommenget D (2012) Influences of the tropical Indian and Atlantic Oceans on the predictability of ENSO. *Geophys Res Lett* 39:1
- Gu D, Philander SGH (1997) Interdecadal climate fluctuations that depend on exchanges between the tropics and the extratropics. *Science* 235:805–807
- Halpert MS, Ropelewski CF (1992) Surface temperature patterns associated with the Southern Oscillation. *J Clim* 5:577–593. [https://doi.org/10.1175/1520-0442\(1992\)005<0577:STPAW T>2.0.CO;2](https://doi.org/10.1175/1520-0442(1992)005<0577:STPAW T>2.0.CO;2)
- Ham YG, Kug JS, Park JY (2013) Two distinct roles of Atlantic SSTs in ENSO variability: North tropical Atlantic SST and Atlantic Niño. *Geophys Res Lett* 40:4012–4017
- Hoerling MP, Kumar A, Zhong M (1997) El Niño, La Niña, and the nonlinearity of their teleconnections. *J Clim* 10:1769–1786
- Hong C-C, Li T (2010) Independence of SST skewness from thermocline feedback in the eastern equatorial Indian Ocean. *Geophys Res Lett* 37:L11702. <https://doi.org/10.1029/2010GL043380>
- Hong C-C, Li T, Kug J-S (2008) Asymmetry of the Indian Ocean dipole Part I: observational analysis. *J Clim* 21:4834–4848
- Hu S, Fedorov AV (2018) Cross-equatorial winds control El Niño diversity and change. *Nat Clim Change* 8:798–802
- Jansen MF, Dommenget D, Keenlyside N (2009) Tropical atmosphere–ocean interactions in a conceptual framework. *J Clim* 22:550–567
- Kang I-S, No H-H, Kucharski F (2014) ENSO amplitude modulation associated with the mean SST changes in the tropical central pacific induced by atlantic multidecadal oscillation. *J Clim* 27:7911–7920. <https://doi.org/10.1175/JCLI-D-14-00018.1>
- Kerr RA (2000) A North Atlantic climate pacemaker for the centuries. *Science* 288:1984–1985
- Kessler WS, McPhaden MJ, Weickmann KM (1995) Forcing of Intra-seasonal Kelvin Waves in the Equatorial Pacific. *J Geophys Res Oceans* 100(C6):10613–10631
- Kucharski F, Syed FS, Burhan A, Farah I, Gohar A (2015) Tropical Atlantic influence on Pacific variability and mean state in the twentieth century in observations and CMIP5. *Clim Dyn* 44:881–896
- Lengaigne M, Guilyardi E, Boulanger JP et al (2004) Triggering of El Niño by westerly wind events in a coupled general circulation model. *Clim Dyn* 23:601
- Levine AF, Jin FF (2010) Noise-induced instability in the ENSO recharge oscillator. *J Atmos Sci* 67(2):529–542
- Levine AF, McPhaden MJ, Frierson DM (2017) The impact of the AMO on multidecadal ENSO variability. *Geophys Res Lett* 44:3877–3886
- Levine AF, Frierson DM, McPhaden MJ (2018) AMO forcing of multidecadal Pacific ITCZ variability. *J Clim* 31:5749–5764
- Li T (1997) Phase transition of the El Niño–Southern Oscillation: a stationary SST mode. *J Atmos Sci* 54:2872–2887
- Li T (2006) Origin of the summertime synoptic-scale wave train in the western North Pacific. *J Atmos Sci* 63:1093–1102
- Li T, Hsu P-C (2017) Chap. 5 Dynamics of El Niño–Southern Oscillation in fundamentals of tropical climate dynamics. Springer Atmospheric Sciences, New York. https://doi.org/10.1007/978-3-319-59597-9_4
- Li T, Zhang YS, Lu E, Wang D (2002) Relative role of dynamic and thermodynamic processes in the development of the Indian Ocean dipole: an OGCM diagnosis. *Geophys Res Lett* 29:2110–2113. <https://doi.org/10.1029/2002GL015789>
- Li X, Xie S-P, Gille ST et al (2016) Atlantic-induced pantropical climate change over the past three decades. *Nat Clim Change* 6:275–279
- Liu L, Yu W, Li T (2011) Dynamic and thermodynamic air–sea coupling associated with the indian ocean dipole diagnosed from 23 WCRP CMIP3 Models. *J Clim* 24:4941–4958. <https://doi.org/10.1175/2011JCLI4041.1>
- Lu R, Dong B, Ding H (2006) Impact of the Atlantic multidecadal oscillation on the Asian summer monsoon. *Geophys Res Lett* 33:L24701. <https://doi.org/10.1029/2006GL027655>
- Luther DS, Harrison DE, Knox RA (1983) Zonal winds in the central equatorial Pacific and El Niño. *Science* 222:327–330
- Lübbecke JF, McPhaden MJ (2014) Assessing the twenty-first-century shift in ENSO variability in terms of the Bjerknes stability index*. *J Clim* 27:2577–2587. <https://doi.org/10.1175/JCLI-D-13-00438.1>
- Luo J-J, Zhang R, Behera S, Masumoto Y, Jin F-F, Lukas R, Yamagata T (2010) Interaction between El Niño and extreme Indian Ocean Dipole. *J Clim* 23:726–742
- McCreary JP Jr, Lu P (1994) Interaction between the subtropical and equatorial ocean circulations: the subtropical cell. *J Phys Oceanogr* 24:466–497
- McGregor S, Timmermann A, Stuecker MF, England MH, Merrifield M, Jin F-F, Chikamoto Y (2014) Recent Walker circulation strengthening and Pacific cooling amplified by Atlantic warming. *Nat Clim Change* 4(10):888–892
- Neelin JD, Battisti DS, Hirst AC, Jin FF, Wakata Y, Yamagata T, Zebiak SE (1998) ENSO theory. *J Geophys Res* 103(C7):14261–14290. <https://doi.org/10.1029/97JC03424>
- Philander SGH (1990) El Niño. Academic Press, San Diego, La Niña and the southern oscillation, p 289
- Poli P, Hersbach H, Berrisford P, Dee D, Simmons A, Laloyaux P (2015) ERA-20C deterministic. ERA Report Series 20, European Centre for Medium-Range Weather Forecasts, Reading, UK.
- Rasmusson EM, Carpenter TH (1982) Variations in tropical sea surface temperature and surface wind fields associated with the southern oscillation/El Niño. *Mon Weather Rev* 110:354–384
- Rayner NA, Parker DE, Horton EB et al (2003) Global analyses of sea surface temperature, sea ice, and night marine air temperature since the late nineteenth century. *J Geophys Res* 108:1063–1082
- Rong X, Zhang R, Li T (2010) Impacts of Atlantic SST anomalies on the Indo-East Asian summer monsoon-ENSO relationship. *Chin Sci Bull* 55:1397–1408
- Rong X, Zhang R, Li T, Su J (2011) Upscale feedback of high-frequency winds to ENSO. *Q J R Meteorol Soc* 137:894–907
- Ropelewski CF, Halpert MS (1989) Precipitation patterns associated with the high index phase of the Southern Oscillation. *J Clim* 2(3):268–284
- Roulston MS, Neelin JD (2000) The response of an ENSO model to climate noise, weather noise and intraseasonal forcing. *Geophys Res Lett* 27:3723–3726
- Saenko OA, Schmittner A, Weaver AJ (2004) The Atlantic–Pacific seesaw. *J Clim* 17(11):2033–2038
- Solman S, Menéndez C (2002) ENSO – related variability of the Southern Hemisphere winter storm track over the eastern Pacific–Atlantic sector. *J Atmos Sci* 59:2128–2140
- Sooraj KP, Kim D, Kug J-S, Yeh S-W, Jin F-F, Kang I-S (2009) Effects of the low frequency zonal wind variation on the high frequency atmospheric variability over the tropics. *Clim Dyn* 33:495–507
- Sung MK, An SI, Kim BM, Kug JS (2015) Asymmetric impact of Atlantic multidecadal oscillation on El Niño and La Niña characteristics. *Geophys Res Lett* 42:4998–5004. <https://doi.org/10.1002/2015GL064381>
- Timmermann A et al (2007) The influence of a shutdown of the Atlantic meridional overturning circulation on ENSO. *J Clim* 20:4899–4919
- Timmermann A, An SI, Krebs U, Goosse H (2005) ENSO suppression due to weakening of the North Atlantic thermohaline circulation. *J Clim* 18:3122–3139
- Trenberth KE, Shea DJ (1987) On the evolution of the Southern Oscillation. *Mon Weather Rev* 115(12):3078–3096. [https://doi.org/10.1175/1520-0493\(1987\)115<3078:OTEOTS>2.0.CO;2](https://doi.org/10.1175/1520-0493(1987)115<3078:OTEOTS>2.0.CO;2)
- Trenberth KE, Shea DJ (2006) Atlantic hurricanes and natural variability in 2005. *Geophys Res Lett*. <https://doi.org/10.1029/2006GL026894>

- Uppala SM, Kållberg P, Simmons A, Andrae U, Bechtold V, Fiorino M, Gibson J, Haseler J, Hernandez A, Kelly G et al (2005) The ERA-40 reanalysis. *Q J R Meteorol Soc* 131(612):2961–3012
- Vecchi GA, Harrison DE (2000) Tropical pacific sea surface temperature anomalies, El Niño, and equatorial westerly wind events. *J Clim* 13:1814–1830
- Wang B (1995) Interdecadal changes in El Niño onset in the last four decades. *J Clim* 8:267–285
- Wang B, An SI (2002) A mechanism for decadal changes of ENSO behavior: roles of background wind changes. *Clim Dyn* 18:475–486
- Wang C et al (2014) A global perspective on CMIP5 climate model biases. *Nat Clim Change* 4:201–205. <https://doi.org/10.1038/nclimate2118>
- Wang C, Kucharski F, Barimalala R, Bracco A (2009) Teleconnections of the Tropical Atlantic to the Tropical Indian and Pacific Oceans: a review of recent findings. *Meteorol Z* 18(4):445–454. <https://doi.org/10.1127/0941-2948/2009/0394>
- Wang C, Liu H, Lee SK, Atlas R (2011) Impact of the Atlantic warm pool on United States landfalling hurricanes. *Geophys Res Lett*. <https://doi.org/10.1029/2011GL049265>
- Wang L, Li T, Zhou T (2015) Effect of high-frequency wind on intra-seasonal SST variabilities over the mid-latitude North Pacific region during boreal summer. *Clim Dyn* 45:2607–2617. <https://doi.org/10.1007/s00382-015-2496-2>
- Williamson MS, Collins M, Drijfhout SS, Kahana R, Mecking JV, Lenton TM (2018) Effect of AMOC collapse on ENSO in a high resolution general circulation model. *Clim Dyn* 50:2537–2552
- Wittenberg AT (2009) Are historical records sufficient to constrain ENSO simulations. *Geophys Res Lett* 36:L12702. <https://doi.org/10.1029/2009GL038710>
- Xiang B, Wang B, Li T (1990) A new paradigm for predominance of standing Central Pacific Warming after the late 1990s. *Clim Dyn* 41:327–340
- Yu JY, Kao PK, Paek H, Hsu HH, Hung CW, Lu MM, An SI (2015) Linking emergence of the central Pacific El Niño to the Atlantic Multidecadal Oscillation. *J Clim* 28:651–662
- Yu JH, Li T, Tan Z, Zhu Z (2016) Effects of tropical North Atlantic SST on tropical cyclone genesis in the western North Pacific. *Clim Dyn* 46(3):865–877
- Zanchettin D, Bothe O, Graf HF, Omrani N, Rubino A, Jungclaus JH (2016) A decadal delayed response of the tropical Pacific to Atlantic multidecadal variability. *Geophys Res Lett* 43:784–792
- Zhang R, Delworth TL (2007) Impact of the Atlantic multidecadal oscillation on North Pacific climate variability. *Geophys Res Lett* 34:L23708. <https://doi.org/10.1029/2007GL031601>

Publisher's Note Springer Nature remains neutral with regard to jurisdictional claims in published maps and institutional affiliations.